Surface & Coatings Technology 286 (2016) 64–71

Contents lists available at ScienceDirect

Surface & Coatings Technology

journal homepage: www.elsevier.com/locate/surfcoat

Diode laser cladding of Fe-based alloy on ductile cast iron and related interfacial behavior

Zhikun Weng [a], Aihua Wang [a,*], Yuying Wang [a], Dahui Xiong [b], Huiqun Tang [b]

[a] State Key Laboratory of Material Processing and Die & Mould Technology, School of Materials Science & Engineering, Huazhong University of Science & Technology, Wuhan 430074, PR China
[b] Wuhan Huagong Laser Engineering Co., Ltd., Wuhan 430223, PR China

ARTICLE INFO

Article history:
Received 12 September 2015
Revised 6 December 2015
Accepted in revised form 11 December 2015
Available online 12 December 2015

Keywords:
Cast iron
Laser cladding
Interface behavior
V-groove bevel

ABSTRACT

In this research, repairing of V-grooves on ductile cast iron substrates has been successfully completed with diode laser cladding technique using Fe-base self-fluxing alloy powder as the cladding material. The repaired samples are free of any defects such as pores and cracks with appropriate process parameters and the V-groove bevel. The bonding interface behavior at different power levels and the effect of the V-groove bevel on the cracking sensitivity of the coatings have been investigated. Optical microscopy, scanning electron microscopy, energy dispersive microanalysis and X-ray diffraction were used to characterize the cladded layers and bonding interfaces. Microhardness of the repaired samples was evaluated after cladding. The results revealed that good bonding interface with discontinuous fusion zone can be achieved at a lower laser power. The cracking sensitivity of the cladded layer is closely related to the V-groove bevel and the V-groove with larger bevel can be repaired with no cracks and pores. The cladded layers consist of austenite and martensite while some carbides such as Cr_7C_3, Fe_7C_3 and Fe_3C are formed in the bonding interface. Microhardness is rather homogeneous throughout the cladded layers and much higher than that of the substrate.

1. Introduction

Ductile cast iron is widely used as molds, cams, machine tool beds, pistons, etc. in different industries because of its good fluidity, low cast, excellent machinability and good combination of strength and toughness. However, under formidable conditions involving abrasion, compact and various forms of erosion, it is liable to break down, which leads to enormous economic losses. In order to reduce the loss of the damaged components, a lot of conventional repairing methods are widely adopted such as TIG welding [1], shielded metal arc welding [2–4], powder welding [5] and flame spray welding [6,7]. However, these methods have crucial drawbacks, such as being time-consuming, large heat affectation, poor bonding strength, large amount of porosities and cracks, or high dilution and distortion of the substrates. Especially, cracks are liable to be generated at the bonding interface and the heat affected zone as the large heat affectation [5].

To solve this problem, laser cladding technology is an appropriate surface repair technology to be chosen due to the advantages such as high efficiency, high flexibility, and narrow heat affected zone, resulting in a strong metallurgical bond with minimum dilution of the substrate, etc. [8]. In the laser cladding process, high-energy laser beam is focused onto the substrate to create a molten pool, metal powders are simultaneously delivered into the focal zone by the powder delivering nozzles, and then rapidly melted and solidified. A clad is formed with the motion of the laser in the X–Y plane. A uniform coating is obtained by partially overlapping individual clads.

In recent years, laser repairing technology has been conducted by various investigators. Song et al. repaired V-grooves on medium carbon steel substrates with laser cladding forming technology and the mechanical properties of the repaired layers have been greatly enhanced in comparison with those of the substrate [9]. Wen et al. used laser hot wire cladding to repair martensite precipitation hardening stainless steel [10]. The cladded layer is free from any pores or cracks. Furthermore, the tensile strength and impact toughness are respectively 96% and 86% of those of the substrate. Borrego et al. reported the repairing of the base materials used in mold production by Nd-YAG laser. Research showed that the fatigue strength of laser repairing welded joints is significantly weaker than base materials [11]. Laser repairing technology for industrial application has been used in various equipment, but there still exist some difficulties in laser repairing of cast iron components, such as how to eliminate the cracks that are liable to generate at the bonding interface. When the laser heat is absorbed by the substrate, the high carbon concentration on the surface of the cast iron will lead to the generation of brittle ledeburite and carbides [12], which is harmful to the cracking resistance of the coating.

Xu et al. used Nd:YAG laser cladding high speed steel coatings on nodular cast iron rolls [13], and the result showed that a lot of microcracks were generated in the coated layer with the thickness of 0.2 mm. A 1-kW ytterbium fiber laser has been used to clad Ni-based

* Corresponding author.
E-mail address: ahwang@mail.hust.edu.cn (A. Wang).

http://dx.doi.org/10.1016/j.surfcoat.2015.12.031
0257-8972/

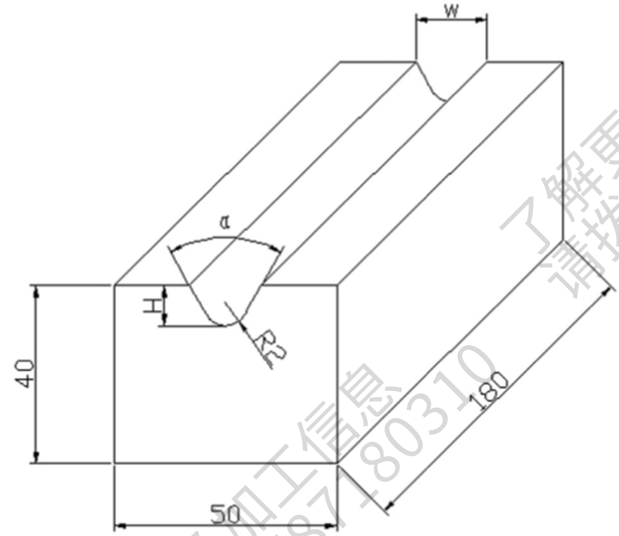

Fig. 1. Schematic of V-groove design.

Table 1
The dimensions of the V-grooves.

	W (mm)	H (mm)	α (°)
A1	16	10	80
A2	20	8.5	100
A3	27.5	8	120

alloy and high speed steel powders on nodular cast iron [14]. Numerous cracks occurred at the interface between the coating and the cast iron, and the cracks can be reduced by preheating the cast iron substrate with the laser beam. In order to eliminate the cracks at the interface of the repair weldments on ductile cast iron with Ni-based alloy powder by fiber laser cladding, Chandra [15] used laser melting surface pretreatment to reduce the number of graphite nodules on the surface of the specimen. Laser surface processing technology has been used by many researches to improve surface properties of cast iron. Yi et al. designed a dynamic local self-preheating in laser cladding Fe-based alloy powder on gray cast iron with CO_2 laser to reduce the thermal stress and better manage the microstructure [16]. The self-preheated cladded layer exhibits no cracks and pores. Although these surface pretreatment and self-preheating devices can reduce the cracks of the coatings, when considering practical repairing conditions, the complicated shape of the damaged surface region and production efficiency must be taken into consideration.

In this paper, the laser cladding process was carried out using a 3 kW DILAS diode laser. Ferrous metals show high absorptivity to diode laser at a wavelength of 980 nm [17], which can save laser energy and cause very small heat-affected zone on the substrate. Furthermore, the uniform energy distribution of diode laser can provide a smooth heating and cooling cycle during the cladding process, which can reduce the thermal stress and dimensional distortion during the process. These characteristics are beneficial to decrease the cracking sensitivity and other defects. In order to simulate the irregular damaged surface, deep V-grooves with different bevels are designed on the ductile cast iron substrates. Laser multi-layer cladding has been carried out to recover the damaged substrates. Macro-quality and microstructure of the repaired layers, especially the bonding interface structure were investigated.

2. Material and experimental procedure

The substrate used in this investigation was a ductile cast iron QT-500 (3.6 wt.%–3.8 wt.% C, 2.0 wt.% Si, 0.411 wt.% Mn, 0.370 wt.% Cu, and the balance Fe) with the dimension of 180 mm × 50 mm × 40 mm. Fe-based self-fluxing alloy powder (0.1 wt.% C, 14.92 wt.% Cr,

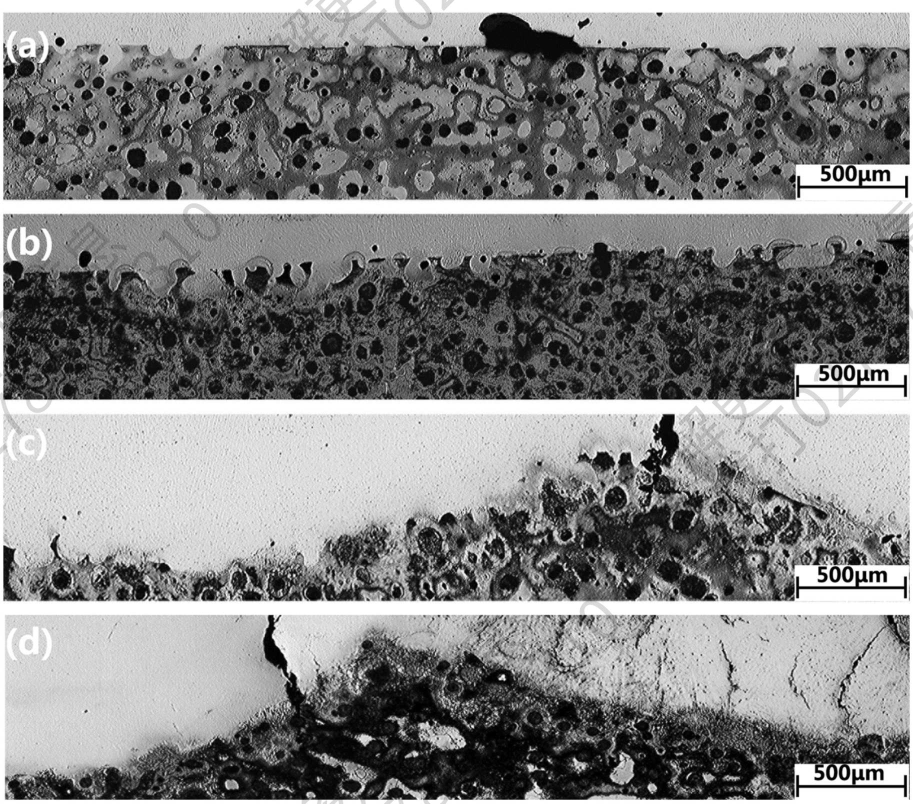

Fig. 2. Morphology of the bonding interface by different laser power ($V_s = 5$ mm/s, $V_p = 11$ g/min). (a) 1.3 kW, (b) 1.5 kW, (c) 1.7 kW, and (d) 1.9 kW.

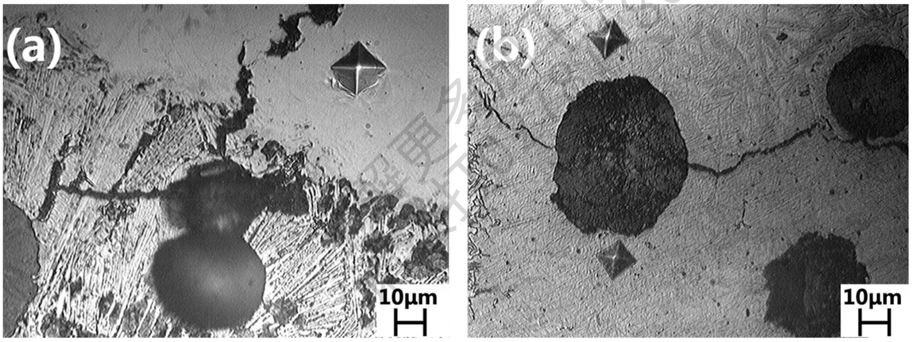

Fig. 3. Microstructure of the crack propagation in (a) interface and (b) heat-affected zone.

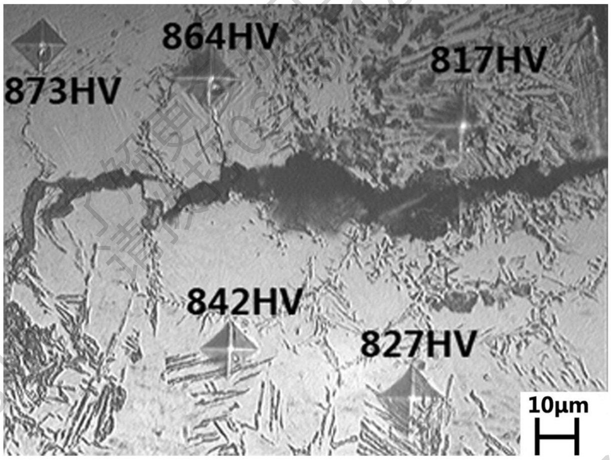

Fig. 4. Microhardness near to the cracks of the bonding interface.

4.4 wt.% Ni, 2.0 wt.% Mo, and the balance Fe) with the particle size in the range of 45–100 μm was selected as the repairing material. The repairing zone was designed as V-grooves up to 10 mm in depth. For the purpose of discussing the effects of the V-groove bevel, three different angles (conducted for A1, A2 and A3) were prepared, as shown in Fig. 1. The dimensions of the V-grooves are listed in Table 1.

Laser cladding was carried out using a diode laser-based cladding system, consisting of a 3 kW high-power diode laser (DILAS SD3000/S) with 980 ± 10 nm wavelength. The off-axial auto-feeding powder equipment was used as the powder feeder and the lateral nozzle was kept at an angle of 45° to the horizontal. Both the laser and the nozzle were fixed to a 6-axis KUKA robot system. Finally, an inert gas, Ar, was used as shielding and powder carrier gas. Prior to repair of the ductile cast iron surface, the crack was removed. The surface of the repairing zone was thoroughly polished with sand paper and all surface contaminants were cleaned with acetone. And the substrate was preheated to 200 °C. Laser processing parameters used in the experiments included the following: laser power (LP) of 1.3–1.9 kW at a scanning speed (V_s) of 6 mm/s and overlapping of 40%–50%, the laser spot diameter was kept constant at 5 mm. The powder delivery velocity (V_p) was set at 9.5–11 g/min.

Laser cladding experiments were firstly carried out on the surface of a planar ductile cast iron plate with different process parameters. Then the laser repairing process was carried out with the optimized parameters. After repairing, liquid dye penetrant testing was used to detect the cracks of the coatings. The microstructure analysis was performed on transverse cross sections of the repaired samples. The section planes were polished and etched with a 4% nital solution. Microstructure characterization was observed and analyzed using optical microscopy (XJL-03) and environmental scanning electron microscope (ESEM Quanta 200 with EDS microanalysis system equipped with light elements). The phase compositions of the repaired samples were determined by X-ray diffraction technology using Cu-K_α radiation at 40 kV and 30 mA (XRD-7000S). Microhardness test was performed using a Vickers-1000 tester.

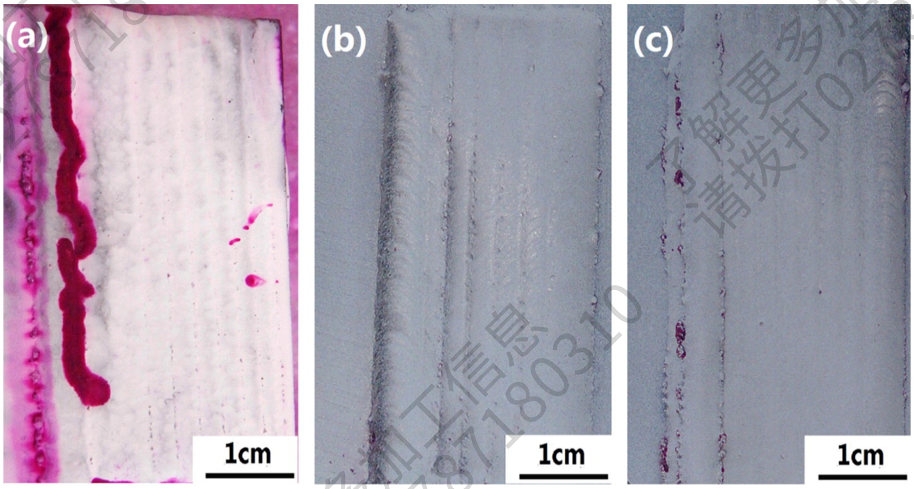

Fig. 5. Liquid penetrant test for cracks inspection. (a) A1, (b) A2, and (c) A3.

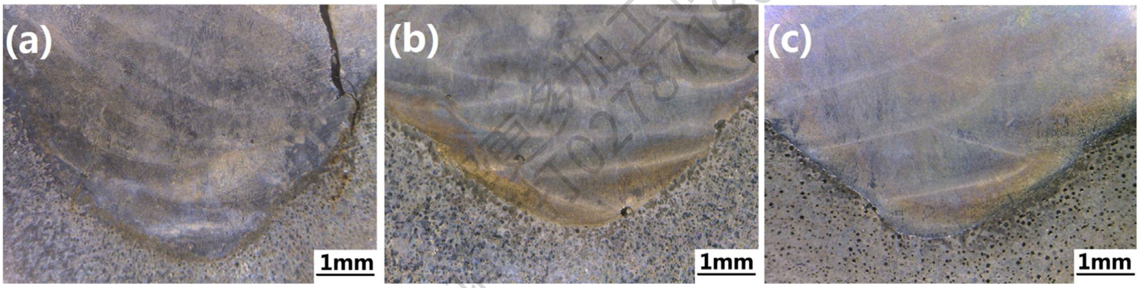

Fig. 6. Morphology of the repaired V-groove zone. (a) A1, (b) A2, and (c) A3.

3. Results

3.1. The effect of laser power on the bonding interface

Fig. 2a–d displays interfacial microstructure between the coating and the substrate at the laser power ranging from 1.3 kW to 1.9 kW ($V_s = 6$ mm/s, $V_p = 11$ g/min). It is obvious that sound interfaces without any porosity and cracks are generated at the laser power of both 1.3 kW and 1.5 kW, as shown in Fig. 2a–b. Higher laser power at 1.7 kW and 1.9 kW results in interfacial cracks. And the higher the laser power, the severer the interfacial cracking is, as shown in Fig. 2c–d. The interfacial cracks in the cross section tend to occur under the concave position of the interface and propagate through the coating into the bonding interface, where a lot of graphite nodules dissolved and no obvious graphite nodule can be seen, as shown in Fig. 2c–d. The crack starts from the graphite nodule which is not completely dissolved on the bottom of the melted zone. It passes through the brittle ledeburite zone and extends into the cladded layer for some distance, as shown in Fig. 3a. And it comes to a stop immediately when it propagates into the graphite nodule, as shown in Fig. 3b. The microhardness near the crack area varies between 800 $HV_{0.1}$ to 900 $HV_{0.1}$, as shown in Fig. 4.

3.2. Effect of the V-groove bevel on the bonding interface

No cracks are observed on the surface of repaired layers for samples A2 and A3. Layers with the smaller bevel, however, developed longitudinal cracks as shown in Fig. 5.

Fig. 6 shows the cross-sectional morphology of the three samples (A1, A2 and A3). It can be seen that A1 has very bad repaired layers, which reveals that obvious cracks are found at the side wall of the V-groove. The V-groove with bigger bevel (up to 120°) is free of cracks at the interface in comparison with A1. For sample A1, the morphology of the interface presents some differences at the bottom and the side wall of the V-groove, as shown in Fig. 7. The fusion degree of the side wall is much higher than that of the bottom. The bonding interface at the bottom of the V-groove is discontinuous, while it becomes continuous at the side wall. The degree of dissolution of graphite nodules at the side wall is much higher than that at the bottom and no obvious graphite nodule is found.

3.3. Microstructure characteristics of the repaired zone

The microstructure of the repaired V-groove zone for A3 is shown in Fig. 8. It can be seen that the distinct fusion bonding interface is obtained between the repaired layers and the substrate. The microstructure of the repaired V-grooves is fine, free of porosities and cracks.

During laser cladding process, a discontinuous bonding interface (namely sawtooth interface) was generated after the laser beam passed across the substrate, as shown in Fig. 8a. A fluctuant microhardness distribution near the bonding interface is observed and the microhardness in the melted zone is much higher than that of the non-melted zone. From Fig. 8b to c, it can be observed that the microstructure in the melted zone consists of ledeburite dendrites and a small proportion of coarse martensite in the bottom. The ledeburite dendrites are surrounded by outer martensite shell. A lot of coarse martensite is formed in the non-melted zone adjacent to the melted zone. The heat-affected zone below the melted zone is characterized by local melting occurring around the graphite nodule. Ledeburite microstructure is formed around the graphite nodule and then surrounded by outer martensite shell as shown in Fig. 9. The microhardness of the ledeburite is about 800 HV to 900 HV and the microhardness of the surrounding martensite is about 500 HV to 600 HV. Fig. 8e to f shows that the microstructure of the cladded layer consists of fine dendrites due to the high cooling rate during laser cladding process. At the overlapped zone, epitaxial dendrites perpendicular to the boundary of two layers can be obtained. There is a coarser zone between two successive layers induced by laser remelting and subsequent slower solidification rate, as shown in Fig. 8f.

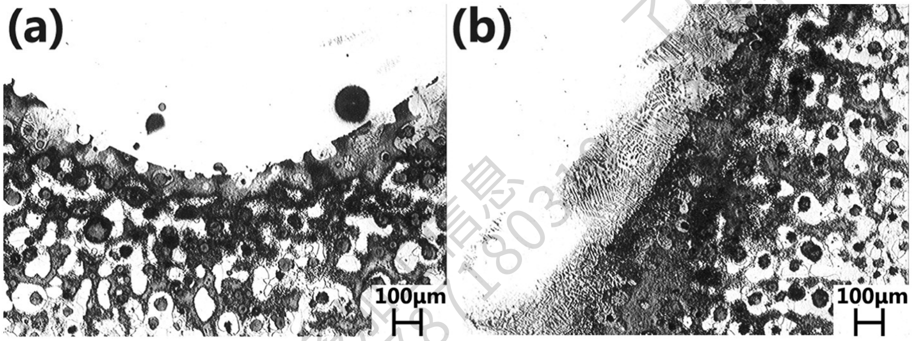

Fig. 7. Morphology of the interface at different location of the V-groove for A1. (a) Bottom and (b) side wall.

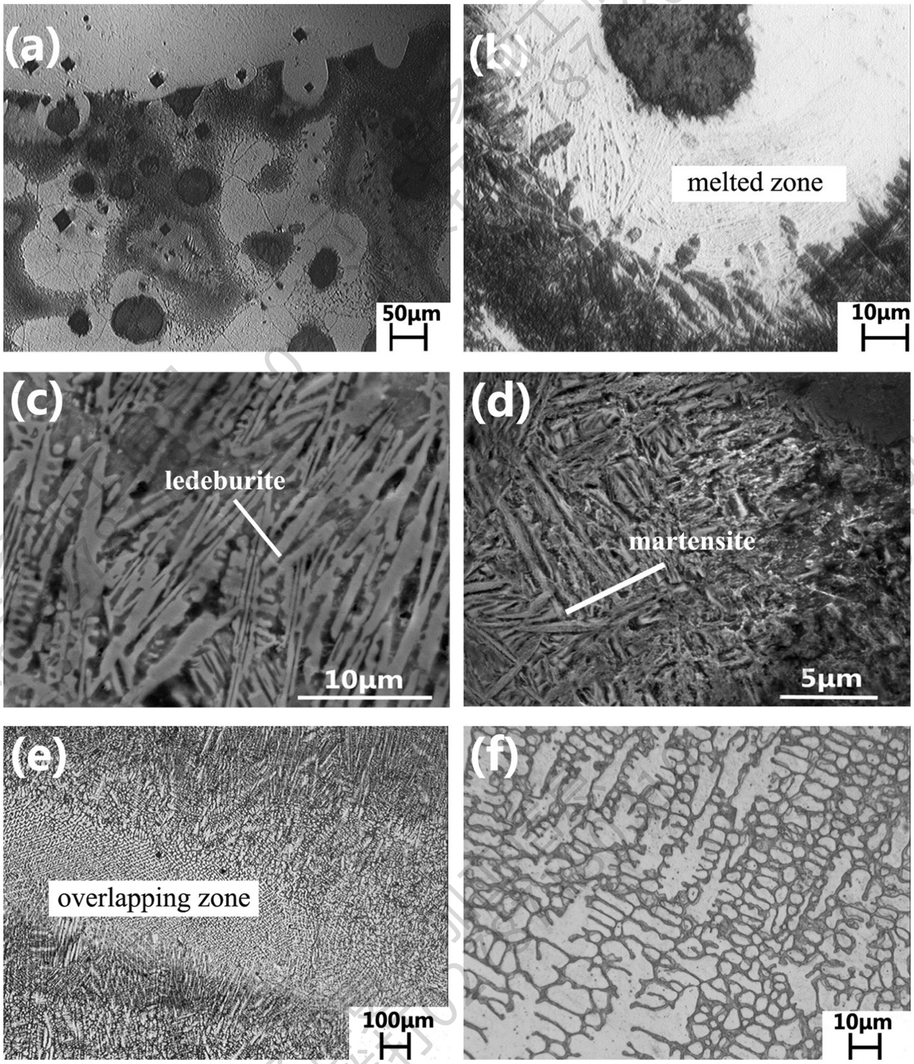

Fig. 8. Micrograph of the bonding interface. (a) Low magnification microstructure of the bonding interface, (b) optical micrograph of the melted zone, (c) SEM image of the melted zone in the interface, (d) SEM image of the non-melted zone in the interface; (e) low magnification microstructure of the cladded layer, and (f) microstructure of the overlapped and epitaxial growth zone.

3.4. X-ray diffraction and EDX analysis

The XRD patterns of the cladded layer and the interface are shown in Fig. 10. As can be seen, the cladded layer only includes austenite and martensite, and no carbide phases exist. Fig. 10b shows XRD pattern of the interfacial zone, it reveals that Cr-rich carbides like Cr_7C_3, Fe_7C_3 and Fe_3C carbides begin to appear at the interfacial zone, which was contributed by the diffusion of alloy elements across the interface. Also, the interfacial zone contains ferrite(Fe) and γ(Fe, Ni) phases.

The concentration profiles of the major elements (Fe, Cr, Ni, Mo and Si) across the bonding interface are exhibited in Fig. 11. Fe and Cr are rich in the melted zone and change rapidly through the interface, and

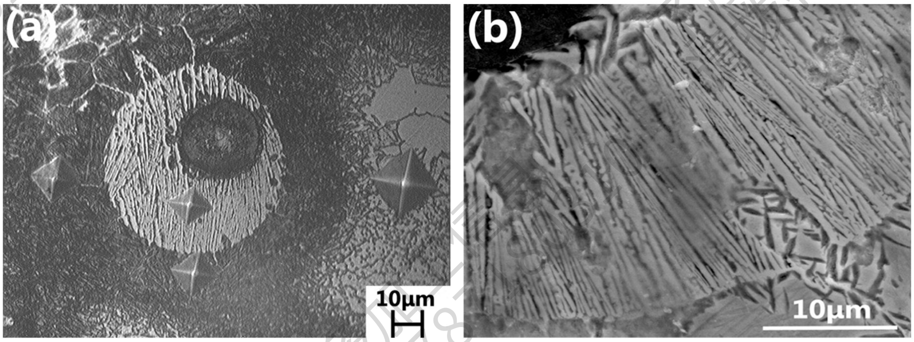

Fig. 9. Microstructure in the heat affected zone. (a) Microstructure around the graphite nodule in the melted zone and (b) SEM image of the ledeburite around the graphite nodule.

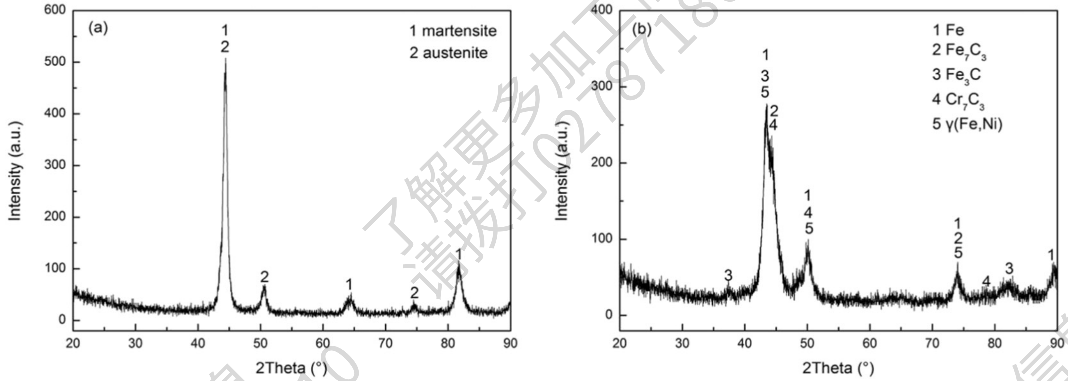

Fig. 10. XRD pattern of repaired sample. (a) Cladded layer and (b) interface.

some elemental inter-diffusions between the cladded layer and the substrate can be observed.

3.5. Microhardness of the repaired layers

The microhardness distributed along the repaired layers varies from 370 to 450 HV, as shown in Fig. 12. It can be seen that the microhardness of the repaired layers is rather homogeneous and much higher than that of the substrate. There is an abrupt increase and fluctuant change at the bonding interfacial zone contributed by the microstructure at the melted zone and the non-melted zone, namely, the melted zone shows much higher microhardness than that of the non-melted zone.

4. Discussion

4.1. Formation mechanism of the interfacial zone

During the laser cladding process, the surface of the substrate was heated above the austenitization temperature, resulting in the transformation of ferrite–pearlite matrix into austenite. At the same time, graphite started to dissolve and the carbon dissolved into austenite microstructure, which resulted in a heterogeneous carbon concentration in the austenite. The diffusivity of carbon into the austenite is a function of temperature and diffusion time [18]. The carbon content of the matrix mainly depends on the distance from the matrix–graphite interface [19]. From basic knowledge of the iron–iron carbide phase diagram, it

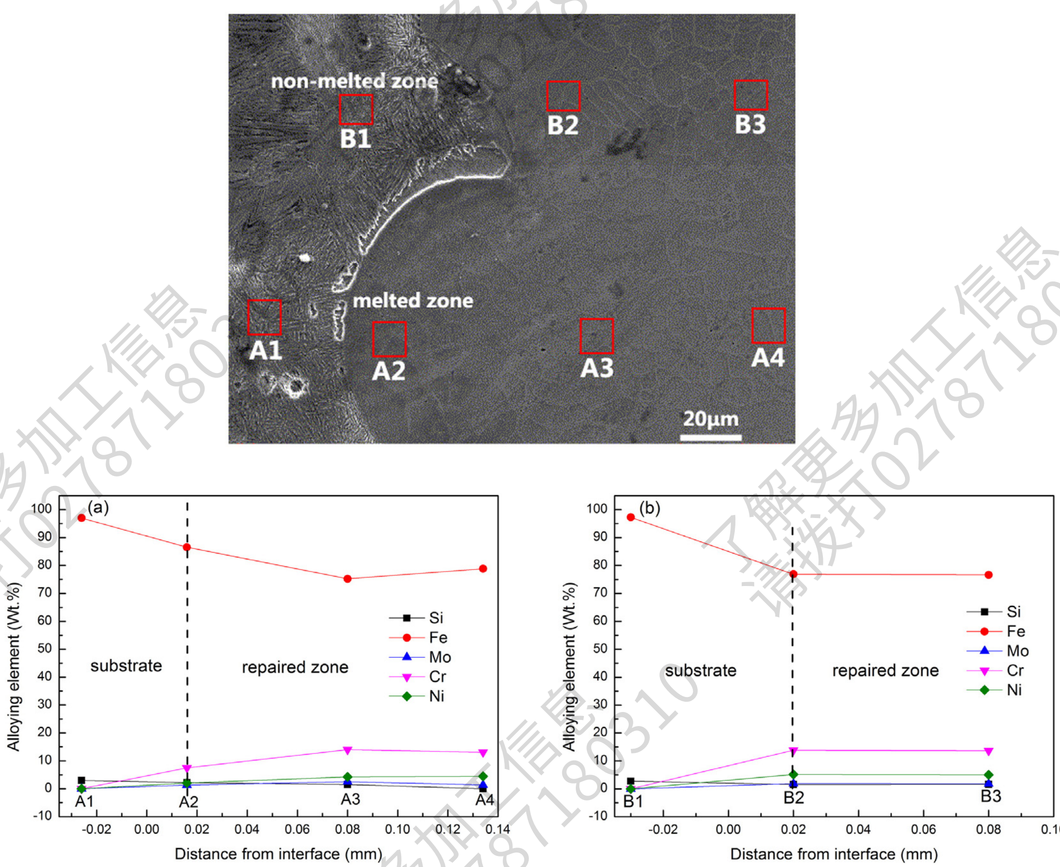

Fig. 11. Element concentration profile for the bonding interface. (a) Element concentration across the melted zone and (b) element concentration across the non-melted zone.

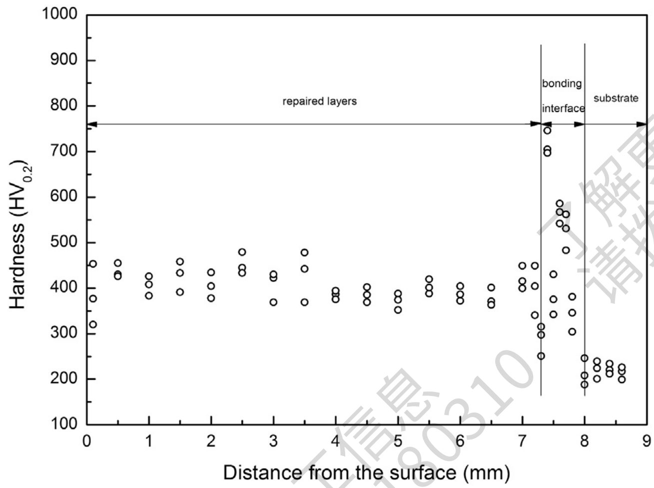

Fig. 12. Microhardness distribution along the cladded layers.

can be seen that the melting-point temperature of the zone where closes to the graphite falls sharply due to the high carbon content there. In the case where the carbon content of the matrix is close to eutectic concentration and the temperature exceeds the eutectic melting temperature, a great deal of ledeburite can be formed in the melted zone. Meanwhile, hard coarse martensite will be formed in the non-melted zone, which is adjacent to the melted-zone.

When the laser power is lower (varies between 1.3 kW and 1.5 kW), the input heat onto the substrate is much lower than at higher laser power. The degree of dissolution of graphite nodules is lower and the carbon concentration in the austenite is extremely heterogeneous, which results in a discontinuous melted zone in the bonding interface, as shown in Fig. 2a–b.

When increasing to a higher power (1.7 kW and 1.9 kW), the degree of dissolution of graphite nodules becomes much higher and more time is available for carbon diffusion. The diffusivity of carbon into the matrix is more homogenous and at a high level, which results in a continuous melted zone in the bonding interface. During the laser cladding process, large thermal stresses caused by the physical differences between the layer and the substrate and the high cooling rate, and the transformation stress caused by the phase transformation in the interfacial zone are produced. After solidification, residual stresses are generated between the clad and substrate. Previous researchers have shown that the clad/substrate interface presents the maximum tensile stress [20]. The residual stress in the interface can be estimated as the following [21]:

$$\sigma = \frac{E_s E_c \alpha_c \Delta T}{E_s + E_c}.$$

where E_s and E_c are the elastic modulus of the substrate and the clad, α_c is the thermal expansion coefficient of the clad, and ΔT is the temperature change after solidification. When $E_s = 1.2 \times 10^5$ MPa, $E_c = 2.1 \times 10^5$ MPa, $\Delta T = 1700$ K, and $\alpha_c = 1.3 \times 10^{-5}$ m/mK, the residual stress would reach 1688 MPa. The high residual stress would cause cracking in the interfacial zone where a continuous of brittle ledeburite are distributed, as shown in Fig. 2c–d. In the diffusion bonding interface, the highest stress concentration is around the graphite nodule area [22], which results in the fact that the graphite nodules become the initiation sites for the cracks along the interface, as shown in Fig. 3.

4.2. Analysis of cracking sensitivity at various bevels of the V-grooves

When multi-layer coatings were laser-cladded into the V-grooves, the angle between the laser beam and level was kept at a constant angle of 80°. During laser cladding process, the continuous multi-layer depositing would result in a heat accumulation on the substrate. In addition, the thermal dissipation becomes more difficult when the V-groove bevel is designed smaller. Therefore, the temperature of the side wall increases much more for the V-groove with smaller bevel. As we know, the laser absorptivity of the cast iron substrate increases when the temperature of the substrate increases [23]. The V-groove with smaller bevel expresses higher degree fusion of the side wall, as shown in Fig. 13.

After multi-layer deposition was completed, the side wall of the V-groove of sample A1 possessed large laser absorptivity, due to its large heat accumulation. Therefore, more energy was absorbed by the surface of the side wall. The higher heat input on the surface of the side wall would cause high degree dissolution of graphite nodules and a continuous ledeburite distribution, as shown in Fig. 13a. In addition, stress concentration could occur in the sharp corner zone between the substrate and the as-cladded layer. The high thermal stress could cause cracking in the interfacial zone where continuous ledeburite distributed and stress concentration could occur, as shown in Fig. 14.

5. Conclusions

(1) The laser power has a significant effect to the quality of the interface between the clad and the substrate. Sound saw toothed interface with no cracks can be achieved at the laser power between 1.3 kW and 1.5 kW with a scanning speed of 6 mm/s and laser spot diameter of 5 mm. With the increase of laser power to higher value, high residual stress would cause cracking in the interfacial zone with continuous ledeburite distributed there.

(2) Microstructure of the cladded layer consists of fine epitaxial dendrites. A characteristic of the bonding interface is that ledeburite formed in the melted zone which was surrounded by the coarse martensite in the non-melted zone. Microhardness is rather homogeneously distributed throughout the repaired layers and much higher than that of the substrate.

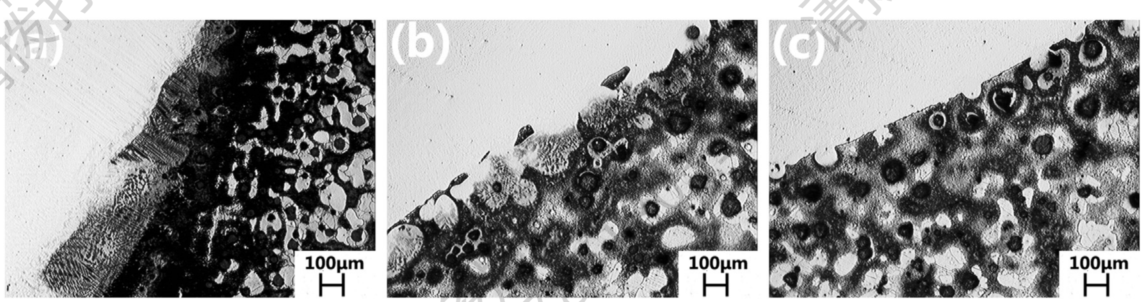

Fig. 13. Morphology of the interface between the cladded layer and the side wall of V-groove. (a) A1, (b) A2 and (c) A3.

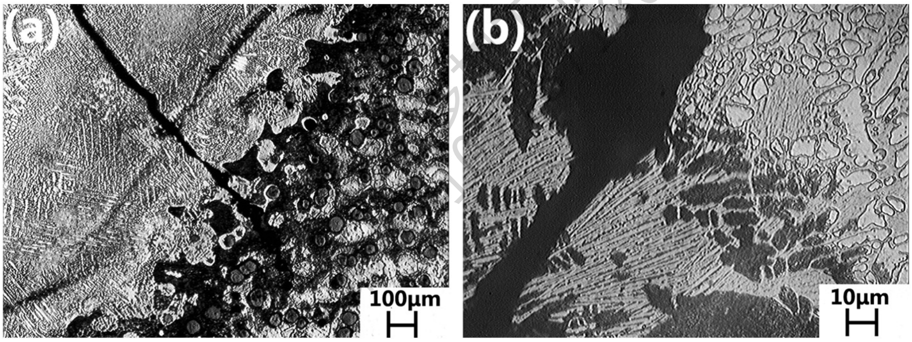

Fig. 14. Cracking at the side wall of the V-groove. (a) Low magnification and (b) high magnification.

(3) Cracking sensitivity of the repaired zone is closely related to the V-groove bevel and laser power. When the laser power is controlled between 1.3 kW and 1.5 kW and V-groove bevel degree is kept at 120°, the repaired multi-layers are free of cracks and pores.

Acknowledgments

The author would like to thank the financial support provided by the National "Twelfth Five-Year" Plan for Science & Technology Support with the contract No. 2012BAF08B02.

References

[1] M.P. Nascimento, et al., Fatigue crack growth investigation on a maintenance welding repair applied on a high responsibility airframe, Prog. Mater. Sci. 3 (2014) 744–749.
[2] E.M. El-Banna, M.S. Nageda, M.M. Abo El-Saadat, Study of restoration by welding of pearlitic ductile cast iron, Mater. Lett. 42 (2000) 311–320.
[3] E.M. El-Banna, Effect of preheat on welding of ductile cast iron, Mater. Lett. 41 (1999) 20–26.
[4] M. Pouranvari, On the weldability of grey cast iron using nickel based filler metal, Mater. Des. 31 (2010) 3253–3258.
[5] F. Malek Ghaini, M. Ebrahimnia, S. Gholizade, Characteristics of cracks in heat affected zone of ductile cast iron in powder welding process, Eng. Fail. Anal. 18 (2011) 47–51.
[6] S.M. Mirhedayatian, et al., Welding process selection for repairing nodular cast iron engine block by integrated fuzzy data envelopment analysis and TOPSIS approaches, Mater. Des. 43 (2013) 272–282.
[7] R. González, et al., Wear behaviour of flame sprayed NiCrBSi coating remelted by flame or by laser, Wear 262 (2007) 301–307.
[8] S. Nowotny, L. Berger, J. Spatzier, 1.18 — Coatings by laser cladding, in: V.K. Sarin (Ed.), Comprehensive Hard Materials, Elsevier, Oxford 2014, pp. 507–525.
[9] J. Song, et al., Rebuilding of metal components with laser cladding forming, Appl. Surf. Sci. 252 (2006) 7934–7940.
[10] P. Wen, Z. Feng, S. Zheng, Formation quality optimization of laser hot wire cladding for repairing martensite precipitation hardening stainless steel, Opt. Laser Technol. 65 (2015) 180–188.
[11] L.P. Borrego, et al., Fatigue behaviour of laser repairing welded joints, Eng. Fail. Anal. 14 (2007) 1586–1593.
[12] G. Sun, et al., Laser surface alloying of C–B–W–Cr powders on nodular cast iron rolls, Surf. Coat. Technol. 205 (2011) 2747–2754.
[13] N.J. Xu, et al., Process optimization and properties of laser cladding high vanadium high speed steel coatings on nodular cast iron, Adv. Mater. Res. 712-715 (2013) 611–614.
[14] Z. Lestan, et al., Laser deposition of Metco 15E, Colmony 88 and VIM CRU 20 powders on cast iron and low carbon steel, Int. J. Adv. Manuf. Technol. 66 (2013) 2023–2028.
[15] C.M. Lin, et al., Repair welding of ductile cast iron by laser cladding process: microstructure and mechanical properties, Int. J. Cast Met. Res. 27 (2014) 378–383.
[16] P. Yi, et al., The effect of dynamic local self-preheating in laser cladding on grey cast iron, Strojniški Vestnik J. Mech. Eng. 61 (2015) 43–52.
[17] S. Barnes, et al., High power diode laser cladding, J. Mater. Process. Technol. 138 (2003) 411–416.
[18] J.T.R. Grum, Comparison of measured and calculated thickness of martensite and ledeburite shells around graphite nodules in the hardened layer of nodular iron after laser surface remelting, Appl. Surf. Sci. 187 (2002) 116–123.
[19] J. Grum, R. Sturm, Microstructure analysis of nodular iron 400-12 after laser surface melt hardening, Mater. Charact. 37 (1996) 81–88.
[20] P. Farahmand, R. Kovacevic, An experimental–numerical investigation of heat distribution and stress field in single- and multi-track laser cladding by a high-power direct diode laser, Opt. Laser Technol. 63 (2014) 154–168.
[21] Y. Liu, et al., Processing, microstructure, and properties of laser-clad Ni alloy FP-5 on Al alloy AA333, Metall. Mater. Trans. B 25 (1994) 425–434.
[22] N. Özdemir, M. Aksoy, N. Orhan, Effect of graphite shape in vacuum-free diffusion bonding of nodular cast iron with gray cast iron, J. Mater. Process. Technol. 141 (2003) 228–233.
[23] A.M. Rubenchik, et al., Temperature-dependent 780-nm laser absorption by engineering grade aluminum, titanium, and steel alloy surfaces, Opt. Eng. 53 (2014) 122506.